Effect of Nature and Particle Size on Properties of Uniform Magnetite and Maghemite Nanoparticles

ARTICLE *in* THE JOURNAL OF PHYSICAL CHEMISTRY C · NOVEMBER 2007

Impact Factor: 4.77 · DOI: 10.1021/jp075133m

4 AUTHORS:

Alejandro G. Roca
Catalan Institute of Nanoscience and Nanote…
46 PUBLICATIONS **1,533** CITATIONS
SEE PROFILE

J. F. Marco
Spanish National Research Council
183 PUBLICATIONS **2,086** CITATIONS
SEE PROFILE

Maria del Puerto Morales
Instituto de Ciencia de Materiales de Madrid
254 PUBLICATIONS **7,979** CITATIONS
SEE PROFILE

C. J. Serna
Spanish National Research Council
226 PUBLICATIONS **9,527** CITATIONS
SEE PROFILE

Effect of Nature and Particle Size on Properties of Uniform Magnetite and Maghemite Nanoparticles

Alejandro G. Roca,*,† Jose F. Marco,‡ María del Puerto Morales,† and Carlos J. Serna†

Instituto de Ciencia de Materiales de Madrid, CSIC, Cantoblanco, 28049 Madrid, Spain, and Instituto de Química Física Rocasolano, CSIC, 28013 Madrid, Spain

Received: July 2, 2007; In Final Form: September 6, 2007

Magnetite nanoparticles with two different sizes, 5 and 17 nm, have been prepared by the decomposition of organic precursors in an organic media in the presence of oleic acid. The particles were characterized by TEM, X-ray diffraction, and IR and Mössbauer spectroscopy to clarify their structural and physicochemical properties. The samples consist of noninteracting magnetite nanoparticles in both cases with a more uniform size distribution and higher crystal order degree than particles of similar sizes prepared by coprecipitation. A controlled heat treatment of the samples in air leads to the transformation of magnetite to maghemite, which can be followed by the appearance of many IR bands forbidden for a spinel structure. In addition to that, an important reduction of saturation magnetization and coercivity at low temperature takes place whenever the oleic acid is preserved. Finally, Mössbauer spectra at different temperatures clearly show the effect of the nature of the iron oxide phase, the particle size, particle interactions, and structural order at the surface in both magnetite and maghemite as a consequence of oleic coating.

Introduction

Magnetic nanoparticles are nowadays the subject of extensive research because of their applications in many different technological areas[1] and, in particular, biomedicine.[2] In this sense, iron oxide is an ideal material because of its biocompatibility and easy removal from the body after its use following natural routes.[3] Iron oxide nanoparticles in the form of colloidal suspensions have already found application as contrast agents for MRI.[4−6] Moreover, properly conjugated with molecules that have an affinity to tumor cells, magnetic nanoparticles could be used for drug delivery, therapy, and regenerative medicine.[7] It should be emphasized that each application requires some specific characteristics of the material and that the structural and physicochemical properties of the nanoparticles determine to a great extent the behavior of the final product when introduced in the body and, therefore, its possible use (i.e., half-life time in the blood and biodistribution).[8,9]

Structural and physicochemical properties of nanoparticulate materials are to a great extent associated with the average particle size and its distribution, particle shape, crystal order, surface characteristics, and presence or absence of bonded molecules, and these parameters could be controlled by a synthesis method.[10,11] In the case of magnetic properties for iron oxide nanoparticles, a strong dependence not only on the particle surface but also on the degree of particle crystallinity has been shown. Thus, for materials with similar particle sizes and size distributions, it is the degree of structural order, at the surface and inside the particles, that determines the different magnetic behaviors.[10]

For biomedical applications, magnetite (Fe_3O_4) would be preferred over maghemite (γ-Fe_2O_3) because of its higher saturation magnetization and susceptibility, which means that it saturates at lower magnetic fields.[12] However, magnetite nanoparticles with sizes below 8 nm are difficult to obtain due to the lack of stabilization against oxidation. Moreover, many studies on larger particles also fail to provide a clear characterization of the precise nature of the magnetite phase due to the difficulty of distinguishing between nonstoichiometric magnetite and a mixture of magnetite and maghemite, forming a core/shell structure, for example. More work should be performed on samples prepared under proper, well-controlled conditions and characterized by complementary techniques.

The decomposition of organic precursor method has yielded markedly improved magnetite nanoparticles with good size control, narrow size distribution, and excellent crystallinity of individual nanoparticles[13−15] in comparison to more traditional methods. Nanoparticles prepared by this method have been proposed for biomedical applications, and they have shown promising performance, in particular, for biomolecule separation and as a NMR contrast agent.[8,16,17]

The aim of this work was to characterize uniform magnetite and maghemite nanoparticles with different sizes prepared by this method, i.e., the decomposition of an organic precursor in organic media and in the presence of oleic acid, which has been shown to be strongly linked to the nanoparticles' surface by covalent bonds.[18] Different and complementary techniques such as TEM, X-ray diffraction, IR spectroscopy, magnetic characterization, and Mössbauer spectroscopy were used for the evaluation of their structural, physicochemical, and magnetic properties.

Mössbauer spectroscopy has been widely used to characterize iron oxide magnetic nanoparticles prepared by different techniques[19−25] since it is one of the most adequate techniques for determining the oxidation degree and cation distribution in Fe_3O_4 nanoparticles. Two main features have been analyzed: the effect of the particle size and the effect of different coatings on the reduction of the magnetic dipolar interactions. In the

* To whom correspondence should be addressed. E-mail: alexgr@icmm.csic.es.

† Instituto de Ciencia de Materiales de Madrid.

‡ Instituto de Química Física Rocasolano.

10.1021/jp075133m CCC: $37.00
Published on Web 11/22/2007

first case, Mössbauer spectra of magnetite particles with different sizes revealed a decrease in the Verwey transition temperature with particle size.[26] For the second feature, the results are more complicated since it has been found that oleic acid coating can lead to a larger relaxation time for magnetite particles of 6 nm but also lead to the opposite effect for maghemite particles of 12 nm.[20,27] In the latter case, the authors claimed that surface effects were neglected and that interparticle interactions decreased due to the coating. It has been established that the anisotropy constant is size dependent due to surface contributions, but it is not clear what happens when the surface is modified by different molecules bonded at different strengths. A particular effort will be devoted in this work to distinguish between magnetite (Fe_3O_4) and maghemite (γ-Fe_2O_3) nanoparticles at the smallest particle size, as well as the study of the effect of the size and coating on the magnetic behavior of these materials.

Experimental Procedures

Synthesis of Nanoparticles. Magnetite nanoparticles of two different sizes were prepared by high temperature decomposition of iron organic precursors following previously reported works.[14,15] The smallest nanoparticles (sample M5) were synthesized using iron acetylacetonate as the precursor and phenyl ether as the solvent. A mixture of 0.71 g of $Fe(acac)_3$ (2 mmol), 2.38 g of 1,2-hexadecanediol (10 mmol), 1.69 g of oleic acid (6 mmol), 1.60 g of oleylamine (6 mmol), and 20 mL of phenyl ether were added to a three-necked flask. Then, the mixture reaction was heated under mechanical stirring, and a flow of nitrogen gas until a temperature of 200 °C was reached. This temperature was kept for 120 min, and then the solution was heated to reflux (254 °C) for 30 min in a nitrogen atmosphere. At the end, the solution was cooled down to room temperature.

The largest nanoparticles (sample M17) were produced using iron pentacarbonyl as the iron precursor and 1-octadecene as the solvent. In the synthesis, 2.56 g of oleic acid (12 mmol) was added to 20 mL of 1-octadecene, and then the mixture was heated. When the temperature reached 100 °C, 0.4 mL of $Fe(CO)_5$ (3 mmol) was added to the reaction flask, and the mixture was heated until reflux (320 °C) and kept at that temperature for 1 h. After that, the solution was left to cool down to room temperature. Then, 0.68 g of *N*-oxide of timethylamine (9 mmol) was added in the flask, heated under nitrogen atmosphere again up to 130 °C, and kept at that temperature for 2 h and finally heated until reflux (320 °C) for 1 h.

In both cases, the powder was obtained by precipitation with ethanol, collected with a magnet, and finally dried under nitrogen flow. A stable suspension of the powder could be obtained when nanoparticles were mixed with 20 mL of hexane and 0.05 mL of oleic acid and sonicated for 5 min. Maghemite nanoparticles (samples G5 and G17) were obtained by heating the corresponding magnetite powders at 150 °C for 3 h in the presence of air.

Characterization. Particle size and shape were studied by TEM using a 200 keV JEOL-2000 FXII microscope. TEM samples were prepared by placing one drop of a dilute suspension of magnetite nanoparticles in hexane on a carbon coated copper grid and allowing the solvent to evaporate slowly at room temperature. The mean particle size (D_{TEM}) and distribution were evaluated by measuring the largest internal dimension of at least 100 particles.

The phase of the iron oxide particles was identified by powder XRD and IR spectroscopy. The X-ray patterns were collected between 10 and 80° (2θ) in a Philips 1710 diffractometer using Cu Kα radiation. The crystal size (D_{XRD}) was calculated from the broadening of the (311) reflection of the spinel structure following standard procedures.[28]

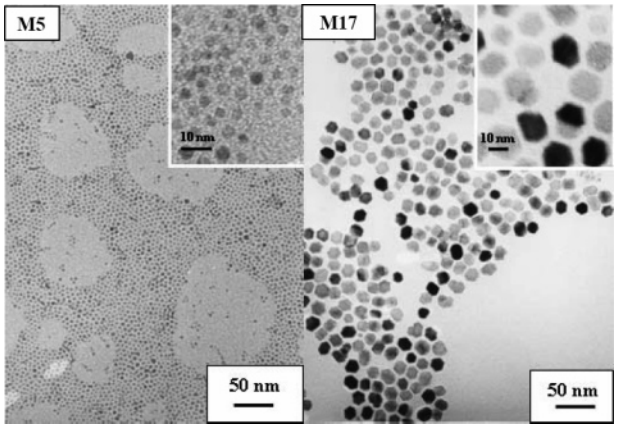

Figure 1. TEM images of magnetite nanoparticles of 5 nm (left) and 17 nm (right).

FTIR spectra were recorded between 3600 and 400 cm^{-1} in a Nicolet 20 SXC FTIR. Samples were prepared by diluting the iron oxide powder in KBr at 2% by weight and compressing the mixture, pressing it into a pellet.

Thermogravimetric analysis of the magnetite powders was carried out in a Seiko TG/ATD 320 U, SSC 5200. The analysis was performed between room temperature and 900 °C at a heating rate of 10 °C/min in an air flow. The weight loss was also registered during the magnetite−maghemite transformation (i.e., heating at 150 °C for 3 h to detect either the weight increase due to the oxidation or the weight loss due to the surfactant elimination).

Magnetic characterization of the samples was carried out in a vibrating sample magnetometer (MLVSM9 MagLab 9 T, Oxford Instruments) at room temperature and 5 K. Magnetization curves were recorded by first saturating the sample in a field of 5 T; then, the saturation magnetization ($\boldsymbol{M}_s$), and the coercive field ($\boldsymbol{H}_c$) were determined for each sample. $\boldsymbol{M}_s$ values were evaluated by extrapolating to infinite field the experimental results obtained in the high field range where magnetization linearly increases with $1/\boldsymbol{H}$.

Transmission Mössbauer spectra between 16 and 298 K were recorded from the two magnetite samples as well as from the two maghemite samples using a conventional constant-acceleration spectrometer equipped with a ^{57}Co (Rh) source and a closed-cycle He cryogenerator (Air Product Inc.). The absorbers were prepared to give an effective thickness of about 10 mg cm^{-2} of natural Fe. The low temperature absorbers were prepared by sandwiching a mixture of powdered sample and vacuum grease between two aluminum foils to ensure good thermal conductivity. All the spectra were computer-fitted. Isomer shifts were referred to the centroid of the spectrum of α-Fe at room temperature.

Results and Discussion

TEM images of the two magnetite samples synthesized by decomposition of organic precursors are shown in Figure 1. These pictures show that the samples consist of nanoparticles uniform in size as it is the main feature of this method.[14,15] Magnetite nanoparticles are isolated one from another by a coating layer of around 2 nm due to steric repulsions of the surface bonded oleic acid chains forming ordered arrays. Nanoparticles produced using iron acetylacetonate as the precursor and phenyl ether as the solvent have a mean average

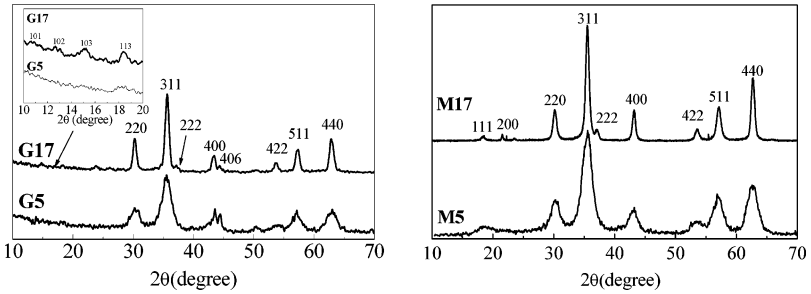

Figure 2. XRD patterns for magnetite and maghemite samples of different sizes.

TABLE 1: Structural and Magnetic Parameters at Room Temperature and 5 K for Magnetite and Corresponding Maghemite Nanoparticles[a]

				magnetic properties			
				5 K		room temp	
sample	D_{TEM} (nm)	P	D_{XRD} (nm)	M_s (emu/g)	H_c (Oe)	M_s (emu/g)	H_c (Oe)
M17	17.0 (2.0)	12	18.0 (1.5)	85	450	76	0
M5	5.0 (1.5)	30	5.8 (1.0)	78	125	64	0
G17				77	370	66	0
G5				76	200	62	0
G5 (400 °C)				66	500	52	0

[a] D_{TEM} is the mean particle size calculated by TEM, P is the degree of polydispersity (standard deviation/mean size), D_{XRD} is the crystal size calculated by X-ray diffraction, M_s is the saturation magnetization, and H_c is the coercivity field.

size of 5.0 ± 1.5 nm (sample M5) and quasi-spherical shapes. When iron pentacarbonyl was used as the precursor and 1-octadecene as the solvent, the mean particle size increased to 17.0 ± 3.0 nm. The formation of larger particles in this case is a consequence of the higher decomposition temperature of the iron precursor, probably due to a delay in the nucleation and therefore in the appearance of a smaller number of nuclei in the initial stages of the reaction.[29] Those nuclei will growth further, helped by the fact that this solvent has a higher boiling point than the other.

X-ray diffractograms for samples M5 and M17 correspond to an inverse spinel structure with lattice parameters 8.38(2) and 8.41(2) Å, respectively, in good agreement with the published magnetite pattern (JCPDS 19−-629) (Figure 2). The broadening of the peaks increases from sample M17 to sample M5, indicating a crystal size decrease following the same trend as the TEM data have shown. Crystallite sizes (D_{XRD}) calculated from Scherrer's equation are in good agreement with TEM size (D_{TEM}), so this means that each particle is a single crystal (Table 1). Further confirmation of the nature of the iron oxide nanoparticles was obtained by IR spectroscopy. The IR spectra for samples M5 and M17 present two main absorption bands at around 585 and 390 cm^{-1}, assigned to the Fe−O stretching modes of the magnetite lattice[30] (Figure 3). Using the space group and point symmetries, group theoretical calculations show the existence of four IR active modes in the vibrational spectra of inverse cubic spinels with two main bands at 570 and 370 cm^{-1} and another two, which are expected to be very weak and only observed at lower wavenumbers.[31] The presence of two bands of weak intensity at 630 and 445 cm^{-1} (Figure 3) indicates some arrangement of cation vacancies generating a lower symmetry structure probably coming from some surface oxidation. Although the particles were synthesized from different precursors and therefore through different mechanisms of formation, the final structure of the particles seems to be the same for both samples, free of defects and impurities.[32]

The oleic acid percentage was around 15% for both samples but was higher for the sample with the smallest particle size, M5, which accounts for the larger surface/volume ratio (Figure 4). DTA analysis reveals that oleic acid is preserved above 200 °C, while at temperatures higher than 500 °C, the transformation to hematite takes place. Moreover, when magnetite particles are heated at 150 °C for 3 h, the sample weight increases by 1% as a consequence of the oxidation of magnetite to maghemite with no change in the oleic acid percentage (Figure 5).

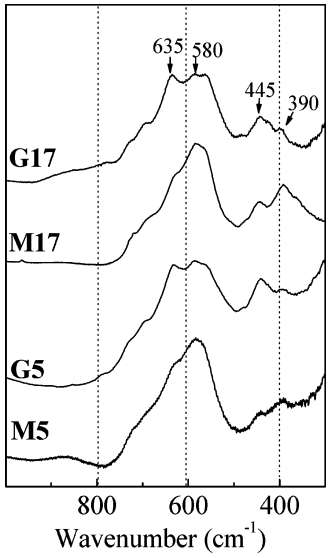

Figure 3. Infrared spectra for magnetite and maghemite samples of different sizes.

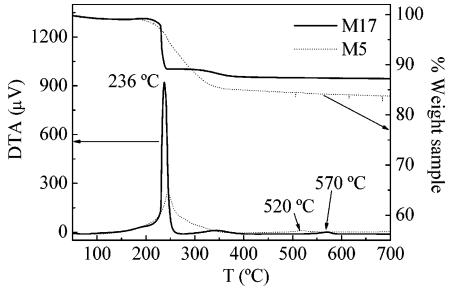

Figure 4. Thermogravimetric and differential thermal analysis of magnetite samples.

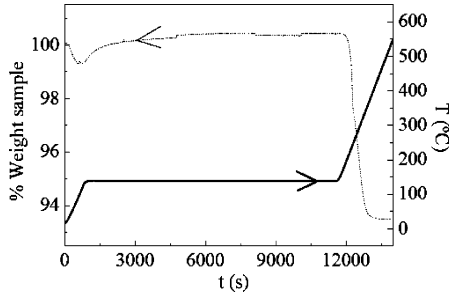

Figure 5. Weight loss during magnetite−maghemite transformation at 150 °C for 3 h.

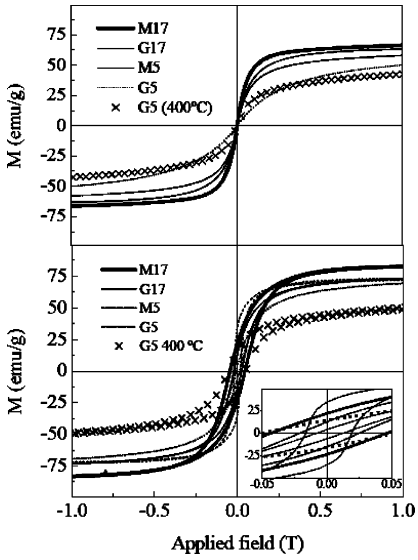

Figure 6. Hysteresis loops at room temperature and 5 K for magnetite and maghemite samples of different sizes.

Maghemite samples, prepared by heating the magnetite powders, present X-ray diffractograms with peaks corresponding to an inverse spinel structure, similar to samples M5 and M17 but with smaller lattice parameters, 8.36(2) and 8.35(2) Å for G5 and G17, respectively (Figure 2). These values are close to the reported values for maghemite (JCPDS 39−-1346). In the low angle region (shown in the inset of Figure 2), superstructure peaks are only observed for sample G17, confirming the transformation to maghemite while the diffractogram for sample G5 is similar to that for sample M5, probably due to the small crystal size. A more spectacular picture of the transition in maghemite is observed with IR spectroscopy (Figure 3). IR spectra for samples G5 and G17 exhibit the two fundamental modes for the spinel structure at 585 and 390 cm^{-1} and many extra lines at 730, 690, 630, 560, 420, and 445 cm^{-1}, which can only be accounted for by assuming a tetragonal symmetry as a consequence of the ordering of the vacancies generated in the oxidation of magnetite to maghemite. The number of bands is, however, less than theoretically predicted for partially ordered (21 active modes) and totally ordered (179 modes) γ-Fe_2O_3.[33] The most striking feature is the enhancement of maghemite bands at 630 and 445 cm^{-1}, which were scarcely visible as shoulders for magnetite.

Magnetization curves for the samples were always reversible at room temperature, suggesting a superparamagnetic behavior that is surprising considering the size of the largest particles, samples M17 and G17 (Figure 6). This result suggests that the presence of oleic acid keeps the particles apart, reducing dipolar interactions. Saturation magnetization values are higher for magnetite and for the biggest particles, as expected. However, at low temperature, $\boldsymbol{M}_s$ values for M17 and M5 were 85 and 78 emu/g, close to those reported for bulk magnetite at room temperature (i.e., 92 emu/g theoretical and 82 emu/g experimental[34] (Figure 6)). In the case of nanoparticles, $\boldsymbol{M}_s$ values of 78 emu/g have been measured for magnetite of 10 nm or larger and 56 emu/g for magnetite particles of 5 nm in diameter, much lower than the value found for sample M5.[26] Again, the oleic acid seems to be responsible for the high $\boldsymbol{M}_s$ values for samples M5 and M17 due to the coordination of the oleic acid molecules to the iron ions at the nanoparticles surface, reducing the spin canting.[18] Consequently, the coercivity is higher for the largest particles since surface effects are neglected, going from 400 to 250 Oe for samples M17 and M5, respectively. Again, opposite behavior was observed for uncoated magnetite particles due to the surface anisotropy contribution, which is dominant at low temperature leading to coercivity values of around 500 Oe for particles of 5 nm.[26]

Maghemite particles showed lower coercivity than the corresponding magnetite according to its lower anisotropy, but the coercivity also changed from 370 to 100 Oe as the particle size was reduced from sample G17 to G5, showing that the oleic acid still diminishes surface anisotropy. A proof of this is the fact that when sample M5 was heated at 400 °C, well above the required temperature to lose oleic acid but lower than that to transform to hematite, the sample presented the largest coercivity value at low temperature (i.e., 500 Oe), in good agreement with the data obtained for bare maghemite nanoparticles.[10] The elimination of oleic acid leads to the reduction in particle separation and the increase in the anisotropy constant due to the surface contribution. Saturation magnetization values at low temperature for maghemite samples G17 and G5 are 76−77 emu/g. The value of $\boldsymbol{M}_s$ for the largest particles is in agreement with the reported values for maghemite nanoparticles of around 12 nm (i.e., 77 emu/g); however, for nanoparticles of 5 nm, much smaller values have been reported (47 emu/g).[10]

It can be concluded that magnetite samples studied in this work consist of uniform and noninteracting nanoparticles. The nature of nanoparticles, either magnetite or maghemite, can be distinguished by XRD for the largest particles, while IR spectra can be used even for particles 5 nm in diameter. However, IR spectroscopy cannot be used to determine the extent of the solid solution because there are no marked changes in the position of the absorption bands with the degree of oxidation.

The Mössbauer spectrum recorded at room temperature for sample M17 (Figure 7) was quite different from that recorded for the 5 nm Fe_3O_4 sample (Figure 9 top) since it was composed of two magnetic sextets and no paramagnetic components were observed. The data suggest that superparamagnetic effects at room temperature were much less important for sample M17 than M5. The spectrum was initially fitted to two discrete sextets, and the obtained Mössbauer parameters are collected in Table 2. We associate the narrower sextet with the larger hyperfine field and the smaller isomer shift with the high spin Fe^{3+} ions occupying the tetrahedral A sites in the spinel-related structure of Fe_3O_4. The broader sextet with the higher isomer shift and the lower hyperfine magnetic field would correspond to the Fe^{3+}/Fe^{2+} ions occupying the octahedral B sites in such a structure.

There are several facts that deserve some comment. First of all, the hyperfine fields observed for the two sextets are lower than those observed for bulk Fe_3O_4. Although is clear that at room temperature the particles are blocked, the broadening of the lines and the lower hyperfine fields reflect their small particle

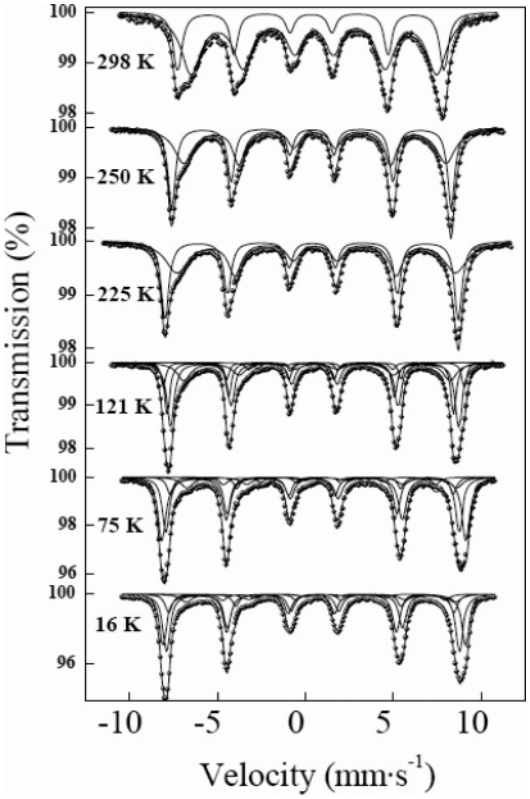

Figure 7. Mössbauer spectra recorded at different temperatures from sample M17.

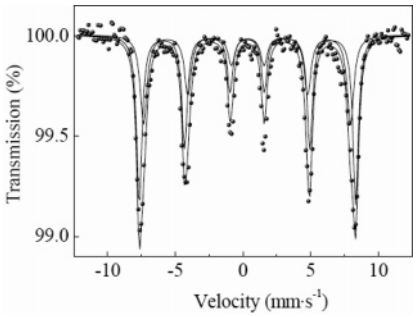

Figure 8. Mössbauer spectra recorded at room temperature from sample G17.

size. So, it is well-known that just below the blocking temperature, superparamagnetic systems show lower hyperfine fields than bulk materials due to the existence of collective magnetic interactions (i.e., to fluctuations of the magnetization direction in directions close to an easy direction of magnetization).[20] Another point that deserves comment is the low isomer shift value observed for the sextet associated with the B sites (0.50 mm s^{-1}) with respect to that shown by bulk, stoichiometric Fe_3O_4 (0.66 mm s^{-1}).[35] This would suggest that the present sample is nonstoichiometric and that it contains less Fe^{2+} than stoichiometric Fe_3O_4 or could be a result of its smaller particle size (it has been reported that isomer shifts in superparamagnetic systems and, specifically, in Fe_3O_4[36] are sometimes lower than those observed in bulk materials). Given that the lines of sextet B are quite broad (ca. 1.14 mm s^{-1}), we also fitted the data using a discrete sextet for the A sites and a hyperfine field distribution for the B sites (Table 2). This type of fit produced a better χ^2 value than that considering two discrete sextets. It can be observed that, with this latter type of fit, the corresponding B/A area ratio is 1.94, which is quite close to that ideally expected, 1.9.[35] Data obtained from the spectra recorded at room

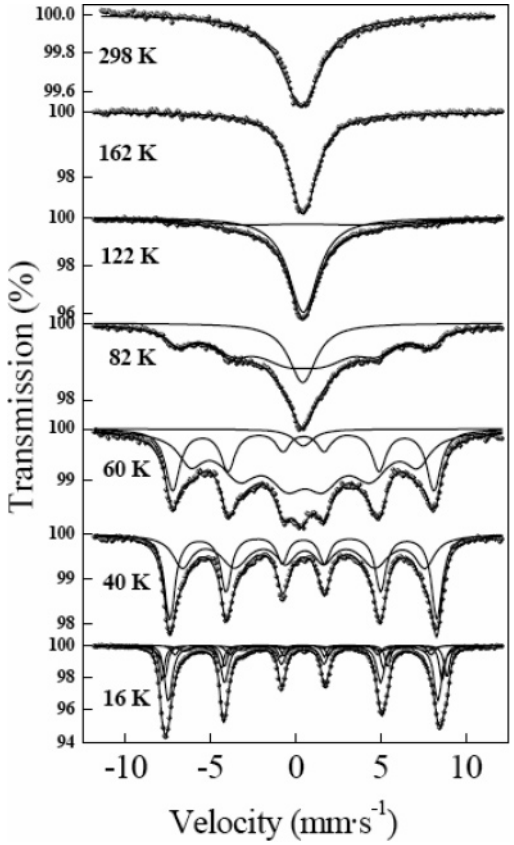

Figure 9. Mössbauer spectra recorded at different temperatures from sample M5.

TABLE 2: Mössbauer Parameters Obtained from Fit of the Spectrum of the 17 nm Fe_3O_4 Sample Using (A) Discrete Lines and (B) Discrete Sextet and HMFD

	component	δ (mm s^{-1})	2ϵ (mm s^{-1})	$\boldsymbol{H}$ (T)	area (%)
A	sextet A	0.32	−0.02	46.9	27
	sextet B	0.50	−0.02	43.0	73
B	sextet A	0.26	0.00	47.3	34
	HMFD (B sites)	0.48	−0.02	38.8[a]	66

[a] $\boldsymbol{H}$ is the average value of the HFMD. The HFMD shows a maximum at 43.8 T.

temperature must be treated with caution given the significant broadening of the spectral lines, which is a consequence of the nanocrystalline character of the sample and of the existence of a particle size distribution.

Mössbauer spectra for sample M17 at 225 and 250 K were very similar (Figure 7). The hyperfine magnetic fields of the A and B components are now much larger than those observed at room temperature (49.3 and 46.3 T, respectively, at 250 K), and the B/A area ratio decreases with respect to that obtained from the room-temperature spectrum. The spectrum recorded at 121 K, that is, close to the temperature at which the Verwey transition occurs in stoichiometric Fe_3O_4, has a different shape and could reflect the onset of some charge ordering in some fraction of the magnetite particles in the vicinity of that transition. The spectra recorded at 75 and 16 K are very similar to those reported for Fe_3O_4 nanoparticles that have already undergone the Verwey transition.[36] Therefore, since a fitting model considering only two discrete sextets did not give satisfactory results, we considered a fitting model with five discrete sextets as has been sometimes considered by other authors.[37,38] The parameters obtained for the spectrum recorded at 16 K are collected in Table 3. The data collected in Table 3 are in reasonable agreement with those recently reported for

TABLE 3: Mössbauer Parameters Obtained from Fit of the 16 K Spectra Recorded from the 17 nm Fe_3O_4 Sample

component	δ (mm s^{-1})	2ϵ (mm s^{-1})	$\boldsymbol{H}$ (T)	area (%)
sextet 1	0.37	−0.00	51.4	34
sextet 2	0.49	0.06	53.5	27
sextet 3	0.65	−0.12	51.7	22
sextet 4	1.04	−0.66	45.8	12
sextet 5	1.13	1.14	40.5	5

TABLE 4: Mössbauer Parameters Obtained from Fit of the 16 K Spectra Recorded from the 5 nm Fe_3O_4 Sample

component	δ (mm s^{-1})	2ϵ (mm s^{-1})	$\boldsymbol{H}$ (T)	area (%)
sextet 1	0.39	−0.02	51.1	20
sextet 2	0.43	0.02	49.1	45
sextet 3	0.47	−0.04	46.7	8
sextet 4	0.62	−0.02	51.4	18
sextet 5	0.77	−0.35	43.9	9

stoichiometric natural magnetite,[37] except for some of the values obtained for the hyperfine magnetic fields corresponding to the sites containing Fe^{2+}. The difference may be related to the nanocrystaline character of our sample and to the lack of spectral resolution. The obtained parameters also show some differences with those obtained from the fit of the spectrum recorded at 16 K from sample M5. As already pointed out by the same authors,[37] the fit of such complicated spectra cannot be unique, and different models are possible leading to similar reliability factors. The B/A area ratio calculated from the relative areas of the different spectral components is, in this case, 1.86.

The spectrum recorded from sample G17 at room temperature is composed of a magnetically split sextet pattern (Figure 8) that was best fitted to two sextets with parameters $\delta_1 = 0.32$ mm s^{-1}, $2\epsilon_1 = 0.01$ mm s^{-1}, $\boldsymbol{H}_1 = 49.6$ T, and area$_1 = 61\%$ and $\delta_2 = 0.33$ mm s^{-1}, $2\epsilon_2 = -0.05$ mm s^{-1}, $\boldsymbol{H}_2 = 47.4$ T, and area$_2 = 39\%$.The parameters of the first sextet are very similar to those shown by bulk maghemite,[39] while the hyperfine magnetic field of the second sextet is lower. We associate this with a fraction of maghemite particles with a particle size large enough as to render a magnetic spectrum at room temperature but not sufficiently large as to give the hyperfine magnetic field of bulk maghemite.

The room temperature Mössbauer spectrum recorded for sample M5 is dominated by a central broad singlet (Figure 9, top), and it is very similar to that shown by other magnetite samples of comparable sizes.[40] A striking feature of this sample is that it shows a very small absorption at room temperature, which is indicative of very loosely bound particles such that their thermal vibrations cause a lowering of the recoil free fraction.[27] We associate this with the presence of oleic acid coating molecules that weakens the mechanical coupling of the particles. In other words, the presence of coating oleic acid molecules causes a very effective separation of the magnetite particles, resulting in a reduction of the mechanical coupling between them and, in all likelihood, also of their magnetic coupling. Figure 9 also shows the Mössbauer spectra recorded at various temperatures from this sample. Between room temperature and 122 K, the spectra are dominated by a broad central singlet, although at 122 K an incipient magnetic component begins to appear in the wings of the spectrum. Finally, the spectrum recorded at 16 K is composed of well-defined magnetic components with no evidence of relaxation (we will later comment on this particular spectrum).

The temperature evolution and shape of the Mössbauer spectra between 162 and 40 K are compatible with the presence of superparamagnetic relaxation. The blocking temperature for sample M5 must be located between 82 and 122 K, much higher than that deduced by magnetic measurements (ca. 8 K[18]), which is in agreement with the different experimental window times.[41] The spectrum recorded at 16 K for sample M5 had a very different shape than that recorded at 40 K, and it is almost identical to those recently reported for dendrite-like self-assembled magnetite nanoparticles in porous silicon.[42] It is, also, not too different in shape to that recorded at that temperature from the M17 sample. Therefore, we used a similar fitting model involving five discrete sextets. The obtained parameters, however, were quite different from those obtained for the M17 sample (Table 4). In general, the hyperfine magnetic fields are smaller in the M5 sample than in the M17 one, which might be a reflection of its smaller particle size or a slightly different stoichiometry. Three out of the five components gave very similar isomer shifts with a weighted average of 0.42 mm s^{-1} and hyperfine magnetic fields ranging from 46.7 to 51.1 T. The sum of the relative areas of these three components amounted to 73% of the total spectral area. The other two sextets, with respective spectral areas of 18 and 9%, presented much higher isomer shifts (0.62 and 0.77 mm s^{-1}, respectively) and corresponding hyperfine fields of 51.4 and 43.9 T. The more divalent character of these two latter components would reflect the onset of some charge ordering in the magnetite particles below the Verwey transition. The quadrupole shifts obtained from the fit for four of the components are close to zero (−0.02 mm s^{-1}), and that of the component with the larger isomer shift is −0.35 mm s^{-1}.

In general, the Mössbauer spectra reported for Fe_3O_4 nanoparticles with particle sizes of the order of 5−6 nm prepared by different methods to that reported here do not show as intense paramagnetic contributions in the vicinity of 80 K. For example, 6 nm Fe_3O_4 particles prepared by chemical coprecipitation[43] and 5 nm Fe_3O_4 particles prepared in the presence of PVA did not show any paramagnetic component in the Mössbauer spectrum at 78 K,[26] while in our case, an important singlet contribution was still observed at 82 K. This significant decrease in the magnitude of the blocking temperatures could be related to the absence of particle interactions and surface anisotropy due to the presence of oleic acid molecules covalently attached to the surface of the oxide particles.[18]

The temperature dependence of the Mössbauer spectra reported here is also quite different from that reported in earlier work performed on suspensions of Fe_3O_4 nanocrystals (6 nm in diameter) in a mixture of acetone and oleic acid.[20] The spectra recorded from these nanocrystals showed very clearly developed magnetic components at 171 and 205 K, and the spectrum recorded at 78 K was composed of very well-defined magnetic sextets.[20] The chemisorption of oleic acid appeared to increase the average superpamagnetic relaxation time, such that the paramagnetic contributions observed at 205 K had a larger intensity in the absence of oleic acid than in the presence of it. This was interpreted as a chemisorption-induced increase in the surface contribution to the magnetic anisotropy constant.[20] The same effect was observed for maghemite particles of 7 nm dispersed in PVA, which also showed an increase of T_B with decreasing concentration of particles in PVA and it was assigned to long range interactions (interparticle magnetic coupling).[44] The results of the present investigation, however, appear to point in the opposite sense, but it should be remembered that the particles are perfectly separated, and therefore, magnetic coupling is diminished. However, oleic acid is covalently attached to the particle surface, and therefore, surface complexation seems to become a predominant factor. Similar results were obtained for maghemite nanoparticles with different

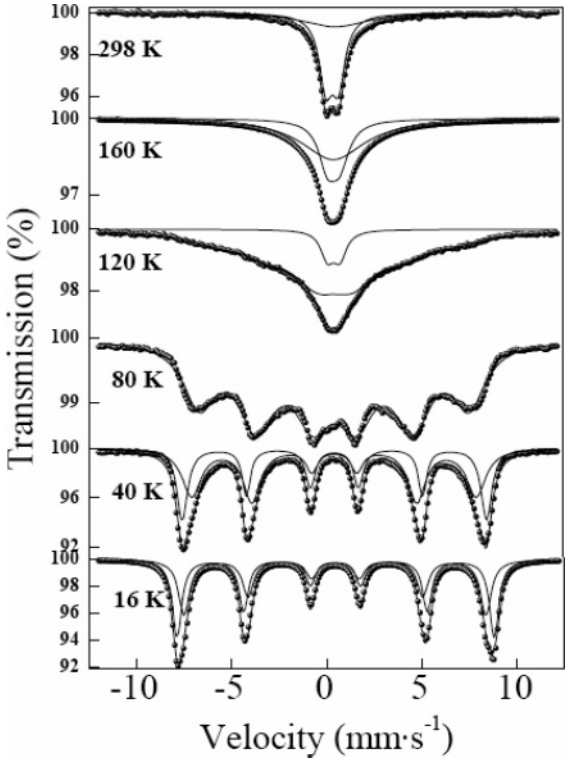

Figure 10. Mössbauer spectra recorded at different temperatures from sample G5.

chelating agents such as phosphates, sulfates, citrate, etc.[45] The pattern evolution was in that case consistent with the chelating affinity in such a way that the stronger the affinity, the lower the blocking temperature.

The Mössbauer spectrum recorded at room temperature from the maghemite nanoparticles of 5 nm (sample G5) consists only of a central paramagnetic doublet, similar to that shown by maghemite nanoparticles,[23] with parameters $\delta = 0.33$ mm s^{-1} and $\Delta = 0.67$ mm s^{-1} (Figure 10). The spectrum shows also considerable broadening at the wings of the doublet, and therefore, a broad band was introduced in the fit to account for such broadening. At 160 K, the spectrum still shows (Figure 10) a large paramagnetic contribution (36%), although, at this temperature, it appears to be much more broadened than at room temperature. The spectrum recorded at 120 K shows a very broad, unresolved magnetic component and a small paramagnetic one (10−15%). At 80 K, the spectrum does not show paramagnetic components but only a broad magnetic one. At 40 K, we observe already a well-defined magnetic sextet pattern that is much narrower in the spectrum recorded at 16 K. This spectrum was fitted considering two hyperfine magnetic sextets of parameters $\delta_1 = 0.46$ mm s^{-1}, $2\epsilon_1 = 0.00$ mm s^{-1}, $\boldsymbol{H}_1 =$ 51.7 T, and area$_1 = 55\%$ and $\delta_2 = 0.44$ mm s^{-1}, $2\epsilon_2 = -0.02$ mm s^{-1}, $\boldsymbol{H}_2 = 49.2$ T, and area$_2 = 45\%$. The shape of the spectra recorded from sample G5 at low temperature resembles that shown by maghemite nanoparticles where interparticle interactions are not negligible.[22]

If we compare the temperature dependence of the Mössbauer spectra of samples G5 and M5, we observe that, at any given temperature above 80 K, the contribution of the magnetic component in the maghemite sample is much larger than in the magnetite sample. In fact, the blocking temperature deduced from the Mössbauer measurements for the maghemite sample would be above 160 K, while, as we have mentioned previous, in the case of the magnetite sample, it would be located between 82 and 122 K. Even more, the shape of the spectra also shows some distinctive features. If we compare the 82 K spectrum recorded from sample M5 and the 120 K spectrum recorded from sample G5 that contain paramagnetic components of about the same intensity, we observe that the magnetic component of sample G5 is much less resolved than that shown by sample M5. A similar comment could be made about the 60 K spectrum recorded from sample M5 and the 80 K spectrum recorded from sample G5. Thus, not only the temperature dependence of both samples (which have similar particle size distributions) is different, but the shape of the respective spectra is also different. Therefore, although the temperature used in this work for the transformation of magnetite into maghemite is not high enough as to lose the oleic acid molecules, the Mössbauer results suggest that the thermal treatment has resulted, anyway, in some reduction of the interparticle distances due to degradation of the oleic acid. Supporting this assumption, TEM images of the maghemite samples are shown in Figure 11, where particles are not arranged forming superstructures as in Figure 1 but forming aggregates where particles are not at the same distance. This is clear for sample G17, and it is not so easy to see for sample G5, which contains a larger amount of oleic acid (Figure 3). Within this context, it is also interesting to note that at room temperature, the absorption of sample G5 is higher than that of sample M5, which suggests that the mechanical coupling of the maghemite particles is higher than that of the magnetite particles. We must recall that, as pointed out by many other authors, in these complex systems, intraparticle interactions (e.g., volume and surface anisotropy and exchange anisotropy) and interparticle phenomena are so closely related, they cannot be easily disentangled.[22,23,46,47] Therefore, the specific origin of the type of magnetic interactions that give the observed Mössbauer behavior would require a more detailed study of the magnetic properties, which is beyond of the scope of the present characterization paper.

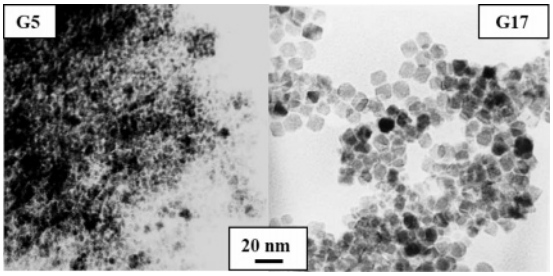

Figure 11. TEM images of maghemite nanoparticles of 5 nm (left) and 17 nm (right).

Conclusion

The data presented here indicate that magnetite nanoparticles of 5 nm prepared by decomposition of organic precursors in an organic media in the presence of oleic acid have a marked superparamagnetic behavior. The superparamagnetic relaxation time at a given temperature between 80 and 120 K is significantly smaller than that shown for Fe_3O_4 particles of comparable sizes but prepared from different synthesis methods. The results point to the absence of interparticle interactions and surface anisotropy. A quite different behavior was observed for the 17 nm magnetite sample. The superparamagnetic character of this sample is much less marked than that shown by the 5 nm sample, although collective magnetic interactions appear to play some role at room temperature. The low temperature data suggest that this sample has undergone already the Verwey transition above 75 K and that it has a stoichiometry close to an ideal one. On the other hand, Mössabuer spectrum for 5 nm

maghemite particles have a different behavior with decreasing temperature than the 5 nm magnetite nanoparticles, suggesting interparticle interactions due to some degradation of the surfactant during heat treatment.

It can be concluded that, when using uniform and noninteracting nanoparticles, it is possible to determine the iron oxide phase, either magnetite and maghemite, for nanoparticles of 17 nm in diameter by XRD and down to 5 nm in diameter by IR spectroscopy, but it is not possible to determine the extent of the oxidation, which can only be resolved by low temperature Mössbauer spectroscopy.

Acknowledgment. This work was supported by the Comunidad Autónoma de Madrid Government under Project S-0505/MAT/0194 and the Ministerio de Educación y Ciencia Institution through the NAN2004-08805-C04-01 and MAT2005-03179 Projects.

References and Notes

(1) Tartaj, P. *Curr. Nanosci.* **2006**, *2*, 43−53.
(2) Berry, C. C.; Curtis, A. S. G. *J. Phys. D: Appl Phys.* **2003**, *36*, 198−206.
(3) Gutiérrez, L.; Lázaro, F. J.; Abadía, A. R.; Romero, M. S.; Quintana, C.; Puerto Morales, M.; Patiño, C.; Arranz, R. *J. Inorg. Biol.* **2006**, *100*, 1790−1799.
(4) Merbach, E.; Tóth, E. *The Chemistry of Contrast Agents in Medical Magnetic Resonance Imaging*; Wiley: New York, 2001.
(5) Bjørnerud, A.; Johansson, L. *NMR Biomed.* **2004**, *17*, 465−477.
(6) Corot, C.; Robert, P.; Idée, J.-M.; Port, M. *Adv. Drug Delivery Rev.* **2006**, *58*, 1471−1504.
(7) Sun, C.; Sze, R.; Zhang, M. *J. Biomed. Mater. Res.* **2006**, *78*, 550−557.
(8) Li, Z.; Wei, L.; Gao, M.; Lei, H. *Adv. Mater.* **2005**, *17*, 1001−1005.
(9) Pankhurst, Q. A.; Connolly, J.; Jones, S. K.; Dobson, J. *J. Phys. D: Appl. Phys.* **2003**, *36*, 167−181.
(10) Morales, M. P.; Veintemillas-Verdaguer, S.; Montero, M. I.; Serna, C. J.; Roig, A.; Casas, L. I.; Martínez, B.; Sandiumenge, F. *Chem. Mater.* **1999**, *11*, 3058−3064.
(11) Tartaj, P.; Morales, M. P.; Veintemillas-Verdaguer, S.; González-Carreño, T.; Serna, C. J. *J. Phys. D: Appl. Phys.* **2003**, *36*, 182−197.
(12) Cullity, B. D. *Introduction to Magnetic Materials*; Addison-Wesley: Reading, MA, 1972.
(13) Rockenberger, J.; Scher, E. C.; Alivisatos, A. P. *J. Am. Chem. Soc.* **1999**, *121*, 11595−11596.
(14) Hyeon, T.; Lee, S. S.; Park, J.; Chang, Y.; Na, H. B. *J. Am. Chem. Soc.* **2001**, *123*, 12798−12801.
(15) Sun, S.; Zeng, H. *J. Am. Chem. Soc.* **2002**, *124*, 8204−8205.
(16) Jun, Y. W.; Huh, Y. M.; Choi, J. S.; Lee, J. H.; Song, H. T.; Kim, S. J.; Yoon, S.; Kim, K. S.; Shin, J. S.; Suh, J. S.; Cheon, J. W. *J. Am. Chem. Soc.* **2005**, *127*, 5732−5733.
(17) Kohler, N.; Fryxell, G. E.; Zhang, M. *J. Am. Chem. Soc.* **2004**, *126*, 7206−7211.
(18) Roca, A. G.; Morales, M. P.; O'Grady, K.; Serna, C. J. *Nanotechnology* **2006**, *17*, 2783−2788.
(19) Woo, K. J.; Hong, J. W.; Choi, S. M.; Lee, H. W.; Ahn, J. P.; Kim, C. S.; Lee, S. W. *Chem. Mater.* **2004**, *16*, 2814−2818.
(20) Morup, S. *J. Magn. Magn. Mater.* **1983**, *39*, 45−47.
(21) Morup, S.; Tronc, E. *Phys. Rev. Lett.* **1994**, *16*, 3278−3281.
(22) Dormann, J. L.; Fiorani, D.; Cherkaoui, R.; Lucari, F.; D'Orazio, F.; Spinu, L.; Noguès, M.; Kachkachi, H.; Jolivet, J. P. *J. Magn. Magn. Mater.* **1999**, *203*, 23−26.
(23) Tronc, E.; Ezzir, A.; Cherkaoui, R.; Chanéac, C.; Noguès, M.; Kachkachi, H.; Fiorani, D.; Testa, A. M.; Grenèche, J. M.; Jolivet, J. P. *J. Magn. Magn. Mater.* **2000**, *221*, 63−79.
(24) Pardoe, H.; Chua-anusorn, W.; St. Pierre, T. G.; Dobson, J. *J. Magn Magn Mater.* **2001**, *225*, 41−46.
(25) Mikhaylova, M.; Kyung Kim, D.; Bobrysheva, N.; Osmolowsky, M.; Semenov, V.; Tsalakos, T.; Muhammed, M. *Langmuir* **2004**, *20*, 2472−2477.
(26) Goya, G. F.; Berquó, T. S.; Fonseca, F. C.; Morales, M. P. *J. Appl. Phys.* **2003**, *94*, 3520−3528.
(27) Morup, S.; Oxborrow, C. A.; Hendriksen, P. V.; Pedersen, M. S.; Hanson, M.; Johanson, C. *J. Magn. Magn. Mater.* **1995**, *140−144*, 409−410.
(28) Azaroff, L. O. *Elements of X-ray Crystallography*; McGraw-Hill: New York, 1968.
(29) Casula, M. F.; Jun, Y. W.; Zaziski, D. J.; Chan, E. M.; Corrias, A.; Alivisatos, A. P. *J. Am. Chem. Soc.* **2006**, *128*, 1675−1682.
(30) Cornell, R. M.; Schwertmann, V. *The Iron Oxides, Structure, Properties, Reactivity, Occurrences, and* Uses; Wiley VCH: Weinheim, Germany, 1996.
(31) Guillot, B.; Jemmali, F.; Rousset, A. *J. Solid State Chem.* **1983**, *50*, 138−145.
(32) Roca, A. G.; Morales, M. P.; Serna, C. J. *IEEE Trans. Magn.* **2006**, *42*, 3025−3029.
(33) Morales, M. P.; Pecharromán, C.; González-Carreño, T.; Serna, C. J. *J. Solid State Chem.* **1994**, *108*, 158−163.
(34) Bate, G. Recording Materials. In *Handbook of Ferromagnetic Materials*; Wohlfarth, E. P., Ed.; North Holland: Amsterdam, 1980; Vol. 2, Ch. 7, p 381.
(35) Vandenberghe, R. E.; Barrero, C. A.; Da Costa, G. M.; Van San, E.; De Grave, E. *Hyperfine Interact.* **2000**, *126*, 247−259.
(36) Morup, S.; Topsoe, H.; Lipka, J. *J. Phys. (Paris)* **1976**, *37*, 287−290.
(37) Doriguetto, A. C.; Fernandes, N. G.; Persiano, A. I. C.; Numes Filho, E.; Grenèche, J. M.; Fabris, J. D. *Phys. Chem. Miner.* **2003**, *30*, 249−255.
(38) Berry, F. J.; Skinner, S.; Thomas, M. F. *J. Phys.: Condens. Matter* **1998**, *10*, 215−1218.
(39) Murad, E.; Johnston, J. H.; Long, G. J. *Iron Oxides and Oxyhydroxides in Mössbauer Spectroscopy Applied to Inorganic Chemistry*; Plenum Press: New York, 1987.
(40) Van Lierop, J.; Ryan, D. H. *Phys. Rev. B: Condens. Matter Mater. Phys.* **2001**, *63*, 644061−644068.
(41) Lima, E., Jr.; Brandl, A. L.; Arelaro, A. D.; Goya, G. F. *J. Appl. Phys.* **2006**, *99*, 83908(1)−83909(10).
(42) Balakrishnan, S.; Gun'ko, Y. K.; Perova, T. S.; Moore, R. A.; Venkatesan, M.; Douvalis, A. P.; Bourke, P. *Small* **2006**, *2*, 864−869.
(43) Morup, S.; Topsoe, H. *J. Magn. Magn. Mater.* **1983**, *2*, 953−954.
(44) Tronc, E.; Prene, P.; Jolivet, J. P.; D'Orazio, F.; Lucari, F.; Fiorani, D.; Godinho, M.; Cherkaoui, R.; Noguès, M.; Dormann, J. L. *Hyperfine Interact.* **1995**, *95*, 129−148.
(45) Tronc, E.; Dormann, J. L. *Hyperfine Interact.* **1986**, *28*, 525−528.
(46) Tronc, E.; Fiorani, D.; Noguès, M.; Testa, A. M.; Lucari, F.; D'Orazio, F.; Grenèche, J. M.; Wernsdorfer, W.; Galvez, N.; Chanéac, C.; Mailly, D.; Jolivet, J. P. *J. Magn. Magn. Mater.* **2003**, *262*, 6−14.
(47) Fiorani, D.; Testa, A. M.; Tronc, E.; Lucari, F.; D'Orazio, F.; Noguès, M. *J. Magn. Magn. Mater.* **2001**, *226*, 1942−1944.